Toward zero-excess lithium sulfur batteries: a systematic coin cell parameter study

Joshua H. Cruddos[1,2,4], James B. Robinson[1,2,4], Paul R. Shearing[3,4], Alexander J.E. Rettie[1,2,4,*]

1. Electrochemical Innovation Lab, Department of Chemical Engineering, University College London, London WC1E 6DH, United Kingdom
2. Advanced Propulsion Lab, Marshgate, University College London, London E20 2AE, United Kingdom
3. The ZERO Institute, University of Oxford, Holywell House, Osney Mead, Oxford OX2 0ES, United Kingdom
4. The Faraday Institution Quad One, Harwell Science and Innovation Campus, Didcot OX11 0RA, United Kingdom

Abstract

Zero-excess lithium (ZEL) or "anode-free" batteries aim to minimise negative electrode material while addressing the challenges associated with handling thin Li metal foils during fabrication. To date, most studies have focused on Li-ion chemistry, with considerably fewer systematic investigations into ZEL-sulfur (ZELiS) cell fabrication and optimization. Here we develop a ZELiS battery, comprising a Li_2S-based composite positive electrode on carbon paper paired with a Ni foil current collector and evaluate the effects of various current collector materials, electrolyte volume to Li_2S mass ratio and C-rate. The developed cells reproducibly achieve an average Coulombic efficiency of 99% from cycles 2 to 200, and a final capacity of 272 mAh g^{-1}_{Li2S} at a C/10 rate. Furthermore, we employ X-ray computed tomography to elucidate the morphological changes and degradation processes occurring within the positive electrode composite, revealing the irreversible loss of Li_2S/S_8 during cycling, which is exacerbated at high rates. These results should be useful in the development of commercially viable ZEL energy storage devices.

1.0 Introduction

Energy storage devices with improved volumetric and gravimetric energy densities beyond Li-ion batteries are essential to mitigate the effects of climate change [1]. One promising candidate is the lithium-sulfur (Li-S) chemistry due to its high theoretical capacity (1,675 mAh g^{-1}) as well as the relative abundance, low cost and favourable geographic distribution of sulfur [2,3] compared to materials used in Li-ion positive electrodes. However, while advances in this technology have been made, widespread commercialisation has been hampered by a range of challenges.

The insulating nature of sulfur and Li_2S necessitates a greater proportion of conductive additives than is required for Li-ion batteries. These typically comprise around 30 wt% of the positive electrode composite, which in turn reduces the energy density of the cell [4,5]. Significant research has been undertaken to increase the active material loading of Li-S cells [6], however this often results in poor electrochemical performance due to low sulfur utilisation and an increase in the polysulfide shuttle effect [7]. Furthermore, the electrochemical performance can be improved by the addition of an excessive mass of conductive carbon to the positive electrode composite and substrate [8,9]. In some instances, as little as 20 wt% sulfur is incorporated into the positive electrode, resulting in a gravimetric capacity too low for practical applications [10].

Additionally, most Li-S cell research is conducted using coin cells which use a Li metal foil as the negative electrode. Although convenient for small scale testing, this approach can equate to a negative-to-positive electrode ratio (N/P ratio) of over 50 [3,5], where a value closer to 1 would be desirable. Li metal's low reduction potential (-3.04 V vs. the standard hydrogen electrode) causes irreversible loss of active S

species during operation: as polysulfides shuttle over to the negative electrode they are irreversibly reduced to solid Li_2S resulting in a loss of active material and negative electrode surface area [11,12]. Furthermore, there are manufacturing challenges involved with the large-scale use of thin Li metal foils, and self-discharge can occur as they are assembled in the charged state [13].

The dynamic nature of the Li metal electrode also poses challenges. When Li deposits it does so inhomogeneously resulting in a very high surface area solid electrolyte interphase (SEI). Side reactions continuously occur between Li-metal and the ether-based electrolyte leading to the consumption of both [14]. Moreover, electrochemically 'dead' Li can be produced which dramatically reduces Li inventory [15]. To mitigate this effect, large excesses of both Li and liquid electrolyte are often used in research laboratories, however this reduces energy density while increasing raw material costs. To realise high-energy-density Li-S batteries, high active-sulfur-contents, low electrolyte-to-sulfur ratios, and ultra-thin Li metal negative electrodes (N/P ratio < 5) are required [1,16].

To minimise the use of Li, an alternative approach involves preparing the positive electrode in the discharged state (i.e., Li_2S) and pairing it with a bare metal current collector (CC) [9,17]. Typically, Ni foil has been the preferred CC choice, however other studies have successfully implemented Cu and stainless steel [13]. Li is reversibly plated and stripped on/from the CC, resulting in an initial N/P ratio of no greater than 1. As all Li is initially contained in the Li_2S composite electrode, manufacturing challenges associated with thin Li metal foils are bypassed (although new ones stemming from Li_2S are noted) as is self-discharge. We term this

configuration a zero-excess Li-S (ZELiS) cell, as opposed to "anode-free" because: (i) anode is poor electrochemical terminology (only true during discharge for secondary cells) and (ii) while the Li negative electrode is not initially present, the cell always operates with positive and negative electrodes.

While many challenges are shared between Li-S and ZELiS formats, e.g., Li metal electrode dynamics, continuous electrolyte consumption and the polysulfide shuttle effect, new issues arise. Since Li_2S is effectively both electronically and ionically insulating [16,17], the use of conductive agents is imperative, with a particular focus on using high surface area carbon to promote the initial oxidation-nucleation reaction of Li_2S [18]. To further improve the kinetics of this reaction, high energy ball milling is routinely employed to reduce the particle size [19]. Even with these efforts, cells must be charged at high overpotentials (> 3.0 V) in the formation cycle to activate Li_2S [19,20]. In addition, the first 5 cycles tend to show poor Coulombic efficiency (as low as 50%) leading to rapid capacity fade. As a result of the N/P ratio being effectively equal to 1, any degradation of the Li negative electrode results in excess S species, making performance closely dependent on the efficiency of reversible Li deposition onto the metallic CC [8,21]. Overall, cell-wide improvements must be made to achieve commercial viability.

So far, studies conducted on similar cell configurations have primarily focused on attempting to improve SEI formation and reversible Li plating/stripping [9,13,15,22,23]. However, cell design and testing parameters used vary widely, making comparison difficult. Thus, a detailed investigation of robust "benchmark" ZELiS cells is warranted to enable rational modifications and achieve the goals of

minimising inactive material content (e.g., conductive additives and binders), low electrolyte volumes and high sulfur loading. Furthermore, the lack of excess Li and rapid capacity fade make it an attractive platform to quickly evaluate the efficacy of cell modifications.

Here, we present a ZELiS coin cell design which exhibits reproducible electrochemical cycling up to 200 cycles. After establishing a robust cell architecture and active material loading value, we systematically varied the CC material and electrolyte volume vs Li_2S loading ratio. Electrochemical testing was used to interrogate the formation process as well as long-term cycling of the optimised cell at various rates, while changes in Li_2S/S_8 particle morphology and distribution were visualised by X-ray micro-computed tomography. We conclude with recommendations and future directions towards commercially relevant ZELiS devices.

2.0 Methodology

All air sensitive manipulations were conducted in an argon-filled glovebox (MBraun, O_2 < 0.5 ppm, H_2O < 0.5 ppm).

2.1 Li_2S ink and positive electrode preparation

Within an Ar-filled glovebox, lithium sulfide powder (Li_2S, 99.9% (metal basis), Fisher Scientific) and conductive carbon additive (C-NERGY super C65, Timcal) were used as received and combined in a zirconia planetary ball milling jar, containing zirconia milling media (Retsch), in a ratio of 7:2, before being dry milled at 500 rpm in 10 min on/off intervals for 18 h in a planetary ball mill (PM 100, Retsch) under inert atmosphere. 10 wt.% styrene co-butadiene (Sigma Aldrich) was pre-dissolved in toluene (anhydrous, Sigma Aldrich) and subsequently wet milled at 500 rpm in 5-min on/off intervals for 2 h, resulting in an overall slurry mixture weight ratio of 70/20/10 for Li_2S/conductive carbon/binder.

The resulting slurry was drop-cast using a pipette (Research Plus, Eppendorf) onto pre-dried, pre-cut 14 mm diameter carbon paper substrates (AvCarb P50, Fuel Cell Store). These were allowed to dry under ambient glovebox conditions overnight, then dried again overnight at 80 °C under vacuum in a Buchi oven (B-585, Buchi).

2.2 Electrolyte preparation

All materials including electrolyte salts, molecular sieves (3 Å, Fisher Scientific), and PTFE syringe filter tips (0.2 µm, Fisher Scientific) were dried under vacuum at 120 ˚C, 220 ˚C and 80 ˚C respectively for three days. Under glovebox conditions, anhydrous solvents were used throughout and dried with the molecular sieves for an additional three days. The solvents were filtered through PTFE syringes into a dry pristine glass vial ready for use. 1 M bis(trifluoromethane)sulfonimide lithium salt (LiTFSI 99% (^{19}F-NMR), Sigma Aldrich) and 0.8 M lithium nitrate ($LiNO_3$,99.99% (metal basis), Sigma Aldrich) were dissolved under stirring

in a 1:1 vol/vol mixture of 1,3-dioxolane (DOL, dried, Sigma Aldrich) and 1,2-dimethoxyethane (DME, dried, Sigma Aldrich) [24–26].

2.3 Materials characterisation

Powder XRD (PXRD) was performed on a SmartLab SE diffractometer (RIGAKU) using a 2 kW Cu source Kα1 and Kα2 (λ = 1.541 and 1.544 Å respectively) operating in Bragg-Brentano mode. Scans were carried out in a 2θ range of 0° to 60° with a step size of 0.01° and a speed of 1.0° min^{-1}. Samples were measured on a zero-background silicon wafer sample holder. Samples for scanning electron microscopy (SEM) were adhered to pin stubs (Agar Scientific) using double sided carbon tape (Fisher Scientific). The SEM images were taken using an EVO-100 (ZEISS) at 15 kV and a working distance of 7 mm.

2.4 Electrochemical measurements and characterisation

Coin cells were prepared inside an Ar-filled glovebox using CR2032-sized coin cell casings (Pi-Kem) containing Li_2S positive electrodes and 15 mm diameter Cu, Ni or stainless steel (Pi-Kem) foils as the current collector negative electrode. Two 0.5 mm and one 0.2 mm thick steel spacers (Pi-Kem) were used alongside a 16 mm diameter Celgard 2400 separator. Electrolyte was pipetted onto the separator prior to the addition of the positive electrode. Cells were electrochemically tested at room temperature using a BioLogic cell cycler (BCS-805, BioLogic). A 4-point connection type holder (CCH-1, BioLogic) was used, and cells were rested for 2 h prior to galvanostatic charge/discharge cycling between cut off voltages of 2.8 and 1.8 V [24]. Electrochemical impedance spectroscopy (EIS) was conducted using a VMP-300 potentiostat (BioLogic) using a 10 mV perturbation voltage over a frequency range of 1 MHz to 0.1 Hz [25].

2.5 X-ray micro-computed tomography

Ex-situ micro-tomography was performed using a lab based micro-CT instrument (Xradia Versa 620, Zeiss). Once charged to the desired the state, the coin cells were transferred to

a glovebox, de-crimped and the Li_2S positive electrodes removed from the casings and dried overnight, under vacuum at 80 °C. A 1 mm diameter sample was hole-punched and positioned within a 1.5 mm diameter PEEK holder (Swagelok). Steel pillars with ferrules were inserted above and below the sample and tightened to ensure the holder was air-tight during measurements.

An optical magnification of 20× was used, and a bin size of 1 was applied to the 2048 × 2048 px CCD detector, resulting in a pixel size of ~375 nm and a field-of-view of ~750 µm. For each set of tomographic data, 501 radiographic projections were obtained at discrete angular steps with an exposure time of 100 to 120 s. The radiographic projections collected were reconstructed using a cone-beam filtered back projection algorithm (XMReconstructor, Zeiss) to produce a set of tomographic slices making up a cylindrical volume.

2.6 X-ray micro- computed tomography data processing

Tomographic images were imported into Avizo (Avizo 2022.1, Thermo Fisher Scientific) for processing and analysis. Sub-volumes were cropped for each tomogram with dimensions of 376 × 376 × 376 cubic voxels. To assist with visualisation, a non-local means filter was applied to each tomographic image. Thresholding segmentation was conducted to identify each phase within the positive electrode material. A connected objects image was computed as a 16-bit file to isolate Li_2S and S images, with additional sieve analysis completed to exclude particles less than 4 cubic voxels (<1.50 μm particle size).

3.0 Results and Discussion

3.1 ZELiS baseline cell development

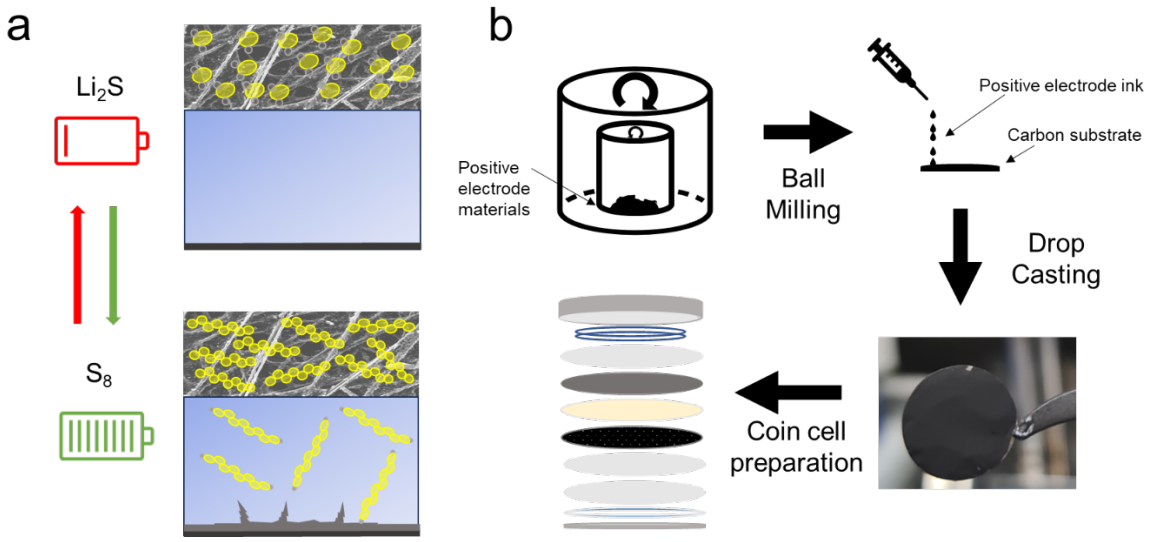

Figure 1. a) Cartoon schematic of the ZELiS during operation. **b)** Procedure for the preparation of Li_2S composite positive electrodes used in coin cells.

Figure 1a illustrates the general design of the ZELiS cell containing a Li_2S/carbon/binder-based positive electrode on carbon paper, a liquid electrolyte and metal current collector. The as-received Li_2S powder was shown to be phase-pure by XRD (Figure S1 in the Supporting Information (SI). Slurry mixtures were prepared in accordance with the method outlined for ink and positive electrode preparation, with a general preparation workflow shown in Figure 1b.

Porous 3D-carbon substrates have commonly been used as positive electrode substrates to facilitate Li_2S activation and cycling. However, it is notable that when included in calculations of the inactive material in the positive electrode composite, this can be ~50 to over 70 wt% [9,13,19,26]. When preparing electrodes, the same carbon substrate was used, and the overall carbon content was targeted to be ~55 wt%.

Ball milling was used to reduce the particle size, improve the activation of Li_2S and make a uniform slurry. The slurry mixture and ball milling procedure were carried out in accordance

with previous studies [19,27,28]. A loading of 2 mg cm^{-2}_{Li2S} was chosen due to inconsistent and poor cell performance at higher loading values. With this fixed positive electrode fabrication procedure and a loading of 2 mg cm^{-2}_{Li2S}, a systematic study was carried out to understand the influence of different current collector materials and electrolyte volume on the cell performance.

3.2 Current collector material

In ZEL cells, the current collector (CC) is especially important as it is the surface on which the Li metal deposits. Three different metallic CCs was investigated based on their commercial availability and existing use in the battery industry: Cu, Ni and stainless steel. Both Cu and Ni have been adopted in previous studies [8,9]. Foils were used as received with no pre-treatment.

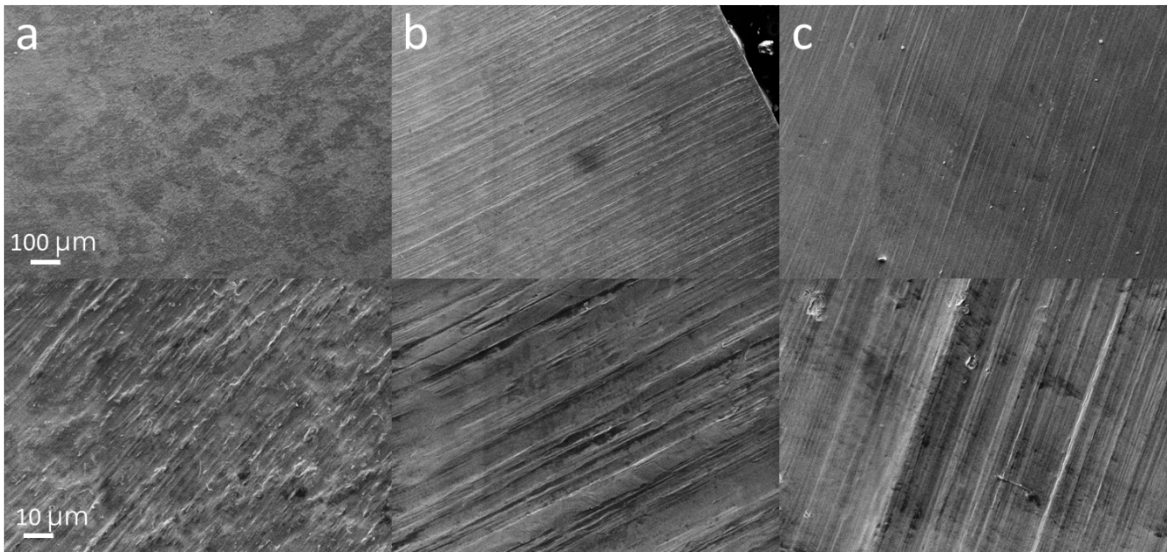

Figure 2. Scanning electron microscopy images of **a)** Cu, **b)** Ni and **c)** stainless steel negative electrode current collectors.

Figure 2 displays the surface morphology of the 3 negative CCs. Generally, all the foils contain slightly pitted surfaces with minor scratches across them, likely from the manufacturing process [29]. The performance of these metals was tested over 50 cycles at a 1C rate shown in Figure 3.

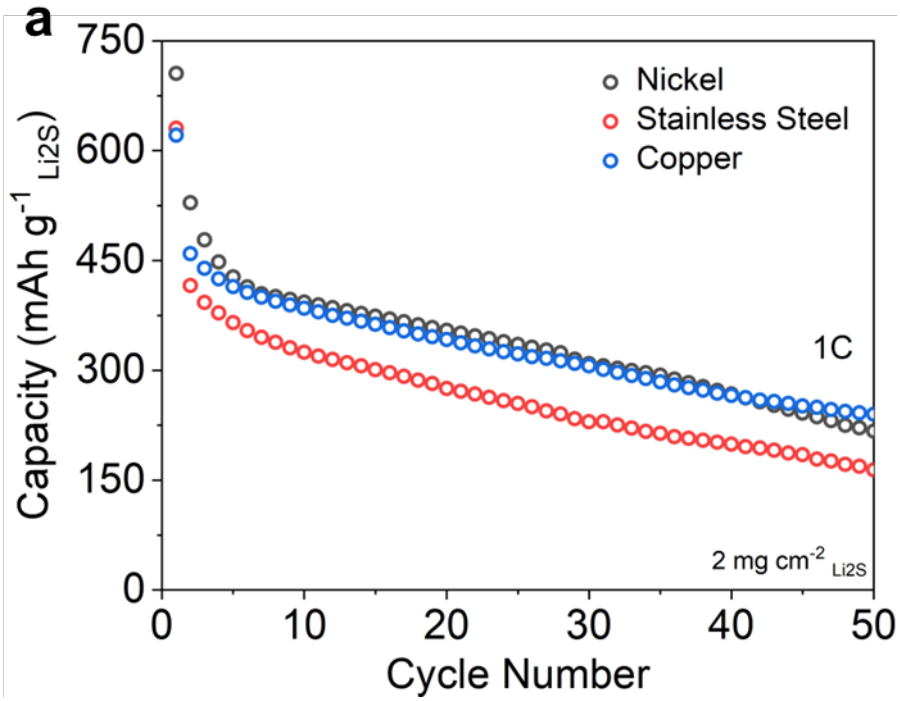

Figure 3. Electrochemical cycling using three different metallic current collectors and an E:S ratio of 15.

Devices using Ni and Cu CCs exhibited similar performance, while stainless steel showed a lower average capacity throughout all 50 cycles. However, the disassembly of multiple cells revealed a dark crusty build up on the Cu CC. In addition, optical microscopy images revealed a similar layer formation on the edge of the Cu CC during the pre-cycle resting (Figure S2 in the SI). Over a short period (< 50 cycles at 1C) this does not appear to affect capacity retention. However, it is consistent with the reactivity of Cu with S species to form copper sulfides over prolonged cycling. Due to the issue with long term cycling stability of Cu in Li-S batteries [30], and the poor performance of the SS, the use of Ni was preferred.

3.3 Influence of electrolyte to active material ratio

The electrochemical performance of five electrolyte to Li_2S mass loading ratios (E:S) is displayed in Figure 4. The range was chosen to bridge the gap between commercialization targets and laboratory research. Exact E:S quantities are defined in Table S1 in the SI.

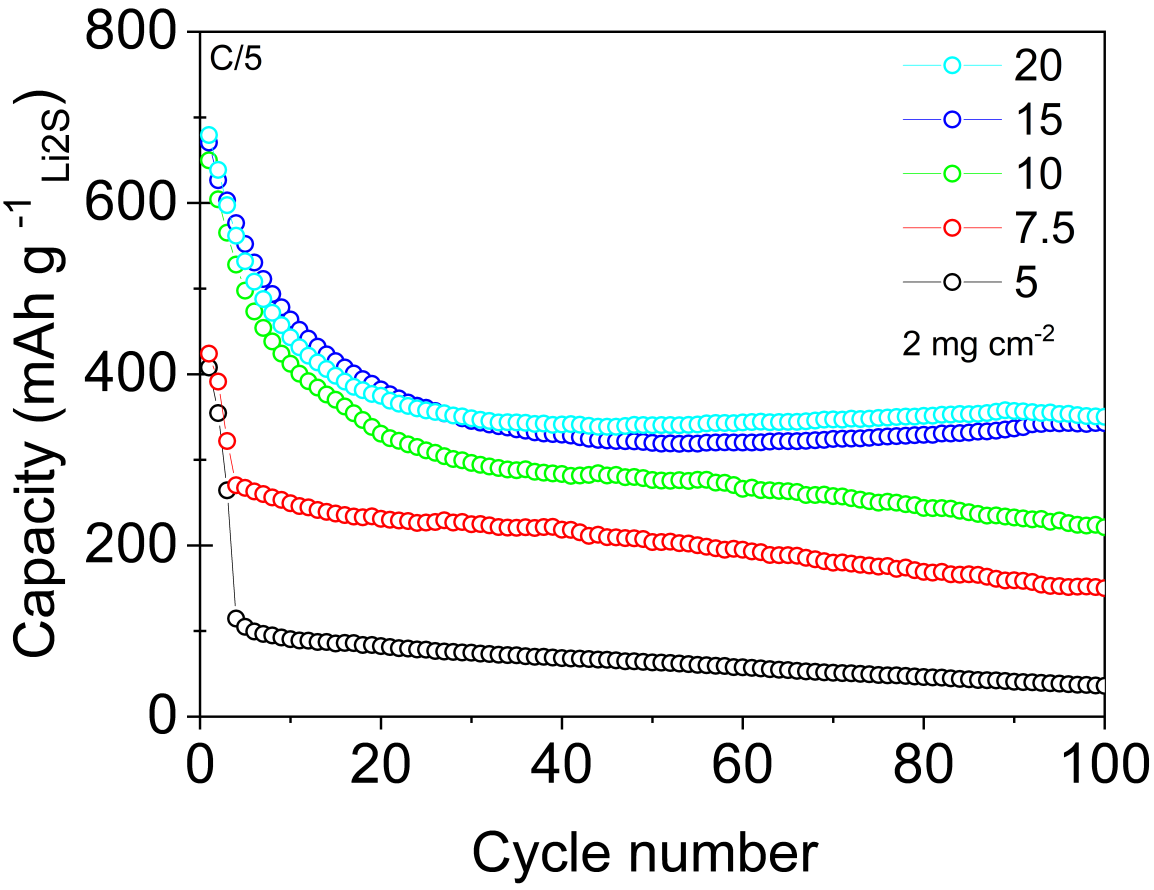

Figure 4. a) Cycling capacity per gram of Li_2S vs cycle number for 5 different E:S (mL g^{-1}_{Li2S}) ratios of electrolyte using a Ni negative CC.

Figure 4 shows that higher quantities of electrolyte resulted in improved capacity retention. An E:S ratio of 5 mL g^{-1} performed worst, only achieving a capacity of 36 mAh g^{-1}_{Li2S} after 100 cycles. At low electrolyte volumes, the electrolyte becomes quickly saturated with polysulfides which, as they undergo the shuttle effect, decrease amount of active sulfur species. This is mainly due to undesirable side reactions between the electrolyte and freshly deposited Li, and the formation of inactive clusters of material within the electrolyte [12,31].

On the other hand, E:S ratios of 15 and 20 mL g^{-1} performed similarly, suggesting >15 mL g^{-1} of electrolyte is not needed. To balance cell performance while minimising electrolyte, an E:S ratio of 15 mL g^{-1} was chosen. Thus, the components and parameters of a baseline cell were established: a 2 mg cm^{-2} Li_2S positive electrode, a Ni foil negative CC, and an E:S ratio of 15 mL g^{-1}.

A clear difference in the initial behaviour between low and high E:S ratios was observed. E:S values ≥ 10 had a positive effect on the initial capacity achieved and retention. This is particularly pronounced in the initial 5 cycles, where E:S = 5 and 7.5 mL g^{-1} exhibited steep drops: falling to 25% and 62% of the initial capacities respectively. In general, excess electrolyte is beneficial for cell cycling [24,32], but there are characteristics of the ZELiS that may compound the expected negative effects of limited electrolyte: (i) the use of Li_2S, which is less electrochemically active and soluble than sulfur, for example, (ii) the porous carbon paper used as the positive electrode substrate which may require more liquid electrolyte for sufficient wetting, and (iii) direct conversion of Li_2S to S_8 being preferred due to the formation of polysulfides being kinetically hindered [20,33].

3.4 Formation cycle characterisation

Figure 5a shows a typical formation cycle of a ZELiS cell. The positive electrode begins as Li_2S with an initial voltage of ~0.0 V. During charging, where Li_2S undergoes conversion to S_8, the voltage rapidly increased to a ~3.0 V plateau before rapidly increasing again up to the 4.0 V cut-off. On discharge, a double plateau was observed, indicating the conventional Li-S multi-stage reduction mechanism, where the mixed product Li_2S/Li_2S_2 has been reported [34,35].

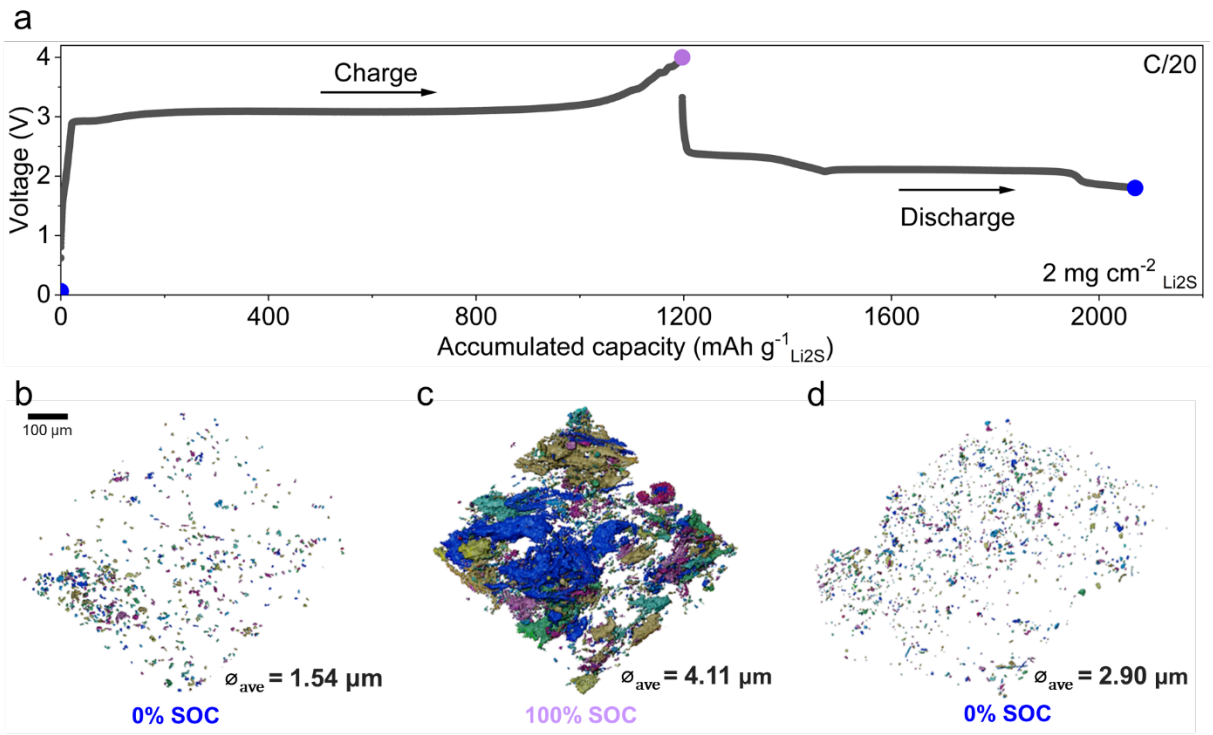

Figure 5. a) Formation cycle of a ZELiS battery. Volume rendering images at 20× of ex-situ Li_2S positive electrode substrates at different states of charge during a formation cycle. **b)** Pristine electrode – Li_2S, **c)** charged S_8 and **d)** discharged Li_2S/Li_2S_2. (scale bar is 100 µm for all three images, $ø_{ave}$ is average particle diameter).

While the formation process is well documented for Li-S positive electrodes [40], detailed studies in a ZELiS set-up are lacking. Specifically, very little is known about the state of the active materials within the carbon CC. To investigate these properties, micro-CT images of

different ZELiS positive electrodes were scanned *ex-situ* at different states of charge (Figure 5b-d).

Li_2S particles with an average diameter ($\varnothing_{ave}$) of 1.54 μm were observed in the pristine electrode (Figure 5b). The small particle size was consistent with a relatively low overpotential for Li_2S conversion (charge voltage plateau at ~3.0 V (Figure 5a)), which has been observed for ball milled materials [27,28]. Good distribution throughout the electrode was seen, which is thought to be also desirable for facile Li_2S activation [19]. Figure 5c shows the positive electrode in the charged state. The morphology of the S_8 differs significantly from the Li_2S particles, showing some S_8 agglomeration and less well dispersed particles generally. The S_8 average particle size was 4.11 µm, significantly bigger than the pristine Li_2S particles. At the end of discharge (Figure 5d), the Li_2S/Li_2S_2 products reformed with similar dispersion to the pristine state, but with an increased average diameter of 2.90 μm.

The changes in particle size and morphology are likely a consequence of S/Li_2S particles re-depositing away from their original location during formation. The underlying mechanisms are complex and not well understood. One candidate is electrolyte 'sink', a phenomenon first reported Zielke *et al.* [36], and subsequently by Yermukhambetova *et al.* [37], where S species precipitate from the electrolyte deep back into the 3D carbon matrix and become less accessible for subsequent cycles leading to a loss of active material and capacity. Additionally, the dissimilar rates at which polysulfides transport in and out of the positive electrode may result in concentration gradients. Studies by Lin et al., and Xu *et al.*, found this to be influential on S particle morphology and size in Li-S cells [34,35]. Both mechanisms support the observation of increasing particle sizes during the initial cycle(s) leading to permanent degradation and loss of active material.

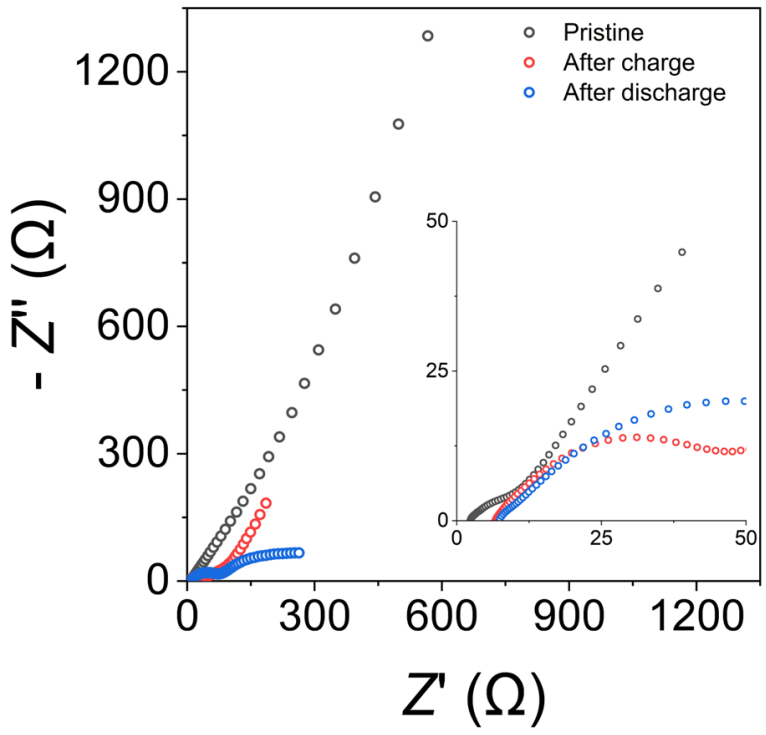

Figure 6. Electrochemical Impedance spectroscopy of a ZELiS formation cycle, with zoomed in inset. Frequency range from 1 MHz to 0.1 Hz.

Figure 6 displays the cell impedance at difference points in the formation cycle. Li-S batteries are known to exhibit numerous (>5) overlapping polarisation processes, requiring advanced analytical techniques, such as distribution of relaxation times analysis [38,39], to deconvolute them. As this is not the focus of our study, here we will qualitatively analyse the EIS of ZELiS cells.

Initially, the pristine case (Li_2S positive electrode|Ni CC) exhibits one, possibly two, semi-circle(s) indicating charge transfer processes followed by a very steep tail in the low frequency region, i.e., the expected blocking electrode behaviour. After the first charge, where a Li electrode has been electrochemically deposited, a low frequency tail with two depressed semi-circles at high frequency were clearly observed. These latter features may indicate several overlapping polarisation processes. Additionally, the real axis intercept shifted to higher impedance values, likely due to the presence of polysulfides in the

electrolyte. Following discharge, depressed semi-circles were observed again but without blocking electrode behaviour. Based on these impedance datasets, the cell does not return to its original state after formation due to the different electrolyte composition and residual Li on the CC [40].

3.5 Effect of C-rate on cycling performance

The effect of C-rate on the optimised ZELiS cell architecture is depicted in Figure 7. Note the good reproducibility over 12 devices (N = 4 for each rate). The highest capacity retention was seen at low C-rates, where 270 mAh g^{-1}_{Li2S} was achieved after 200 cycles at C/10, vs. 110 mAh g^{-1}_{Li2S} at 1C.

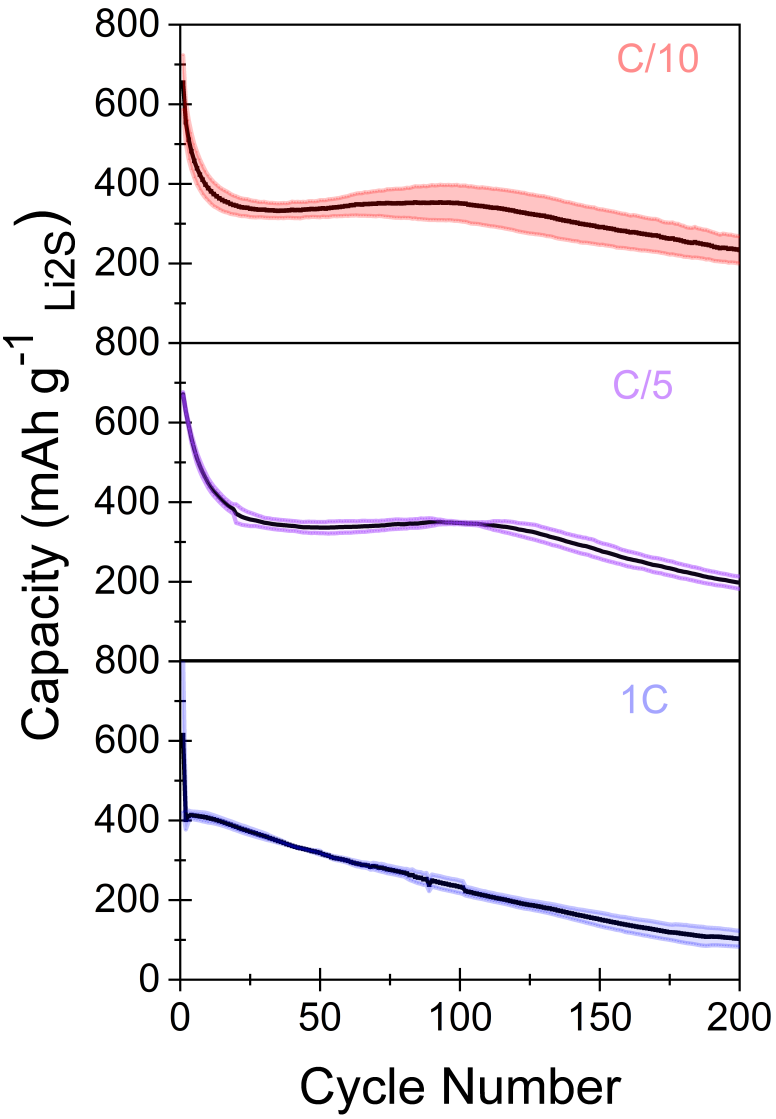

Figure 7. Mean discharge capacity over 200 cycles of several ZELiS cells at C/10, C/5 and 1C rates. The number of repetitions for all C-rates was N = 4 and the shaded area in each indicates ±1 standard deviation. Cells were composed of a 2 mg cm^{-2}_{Li2S} positive electrode, Ni current collector and an E:S ratio of 15 mL g^{-1}.

All cells exhibited a large drop in capacity within the first five cycles. This was most severe at 1C: equivalent to a 50% capacity loss in cycle 1. At slower rates, the capacity decay was still significant but lessened: declining 26% and 31% in cycle 1 for C/5 and C/10 respectively. In these cases, a small increase in capacity followed by a plateau was observed around 100 cycles (Figure 7), before a consistent decline towards cycle number 200.

The initial drop in capacity has been attributed to degradation of the *in-situ* Li negative electrode with contributions also from sulfur inventory losses [26]. The capacity increase observed around 100 cycles may be due to polysulfide reabsorption into the positive electrode [11]. This would indicate that the conversion back to Li_2S/Li_2S_2 on discharge is significantly lower than the reverse process on charge, leading to a steadily increasing concentration of polysulfides in the electrolyte. A dynamic equilibrium between the redox species could allow more active material to slowly become more accessible at later cycles [17]. This is followed by sustained irreversible losses from both electrodes leading to capacity values of ~200 mAh $g^{-1}{}_{Li2S}$ for both C/5 and C/10 rates after 200 cycles. The difference between 1C and the slower C-rates was stark, therefore to better understand the underlying processes, X-ray micro-CT imaging was performed.

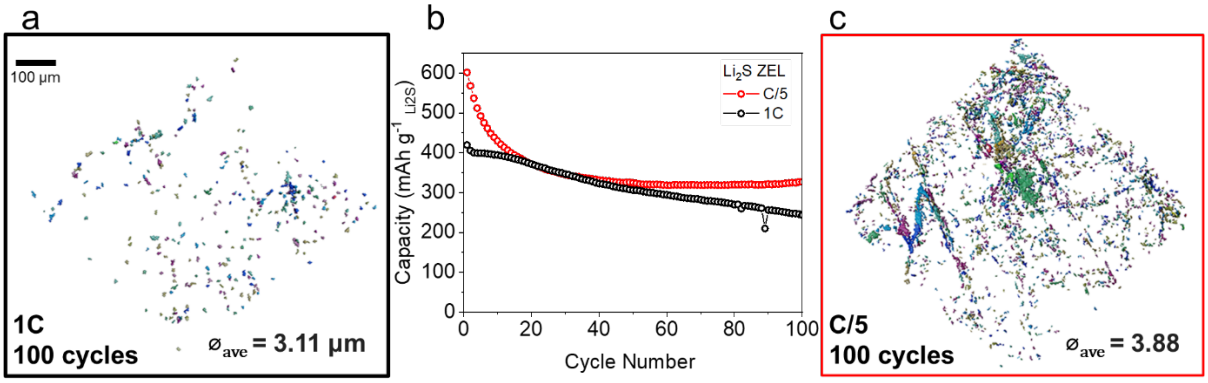

Figure 8. Volume rendering images of *ex-situ* positive electrode substrates after 100 cycles at **a)** 1C **c)** C/5 rates. The corresponding electrochemical cycling data for each C-rate is shown in **b)**. Cells were composed of a 2 mg $cm^{-2}{}_{Li2S}$ positive electrode, Ni

current collector and an E:S ratio of 15. (scale bar is 100 µm for all three images, $ø_{ave}$ is average particle diameter).

Figure 8 displays CT images of positive electrodes following 100 cycles at different (dis)charging rates. At the higher C-rate, there appeared to be substantially fewer Li_2S/S particles and less particle agglomeration. The average particle size was smaller for the 1C rate: 3.11 μm compared to 3.88 μm for C/5. This would indicate the polysulfide shuttle effect is stronger at high C-rates, causing more permanent loss of S species, leaving fewer, smaller particles within the electrode available to react and vice versa. Studies of conventional Li-S cells have shown a similar C-rate-capacity correlation and found the degradation mechanism may show a time dependence [32].

3.6 Recommendations

With the considerations above, this leads to the following recommendations for ZELiS cell research. First, while slurry mixtures often contain low quantities of carbon (<30 wt%), the actual inactive material value can be significantly higher (>70 wt%) due to the commonly used carbon paper substrate. Next phases of research should aim to reduce this (or remove entirely) to improve energy density metrics, by moving to slurry-coated metallic foils for example. Secondly, the electrolyte is an important component of the Li-S chemistry; however, it also contributes the largest weight fraction to the specific energy of a ZELiS cell. Therefore, future work should aim toward E:S < 5 µL mg $^{-1}_{Li2S}$ but this will be challenging, as performance declines drastically as electrolyte volume decreases (Figure 4). However, we note that the removal of the 3D porous substrate, which likely requires excess electrolyte to wet, could be beneficial for performance at lower E:S ratios as well. Electrolytes must be designed to be highly soluble for redox active lithium-polysulfides, ionically conductive and minimize polysulfide shuttling. This has mainly been accomplished by ether-based electrolytes with Li-salts to-date, however other systems, including solid state electrolytes, and functional additives, should be investigated [1,41]. Attempts to improve Li metal

plating and stripping are also important and could be achieved by incorporating thin, ionically conductive artificial SEIs onto the current collector. Finally, the applied pressure is an important component that may be beneficial in improving the cyclability, particularly Li plating and stripping efficiency [42]. This may be more amenable to pouch cell formats, but it is likely like coin cells will remain an important architecture for ZELiS research and development.

Conclusions

In summary, we report a consistent ZELiS cell comprising a Ni negative CC, E:S ratio of 15 mL g^{-1} and active material loading of 2 mg cm^{-2}_{Li2S} in a carbon paper substrate. This configuration achieved ~270 mAh g^{-1}_{Li2S} after 200 cycles at C/10 rate. All cells exhibited substantial capacity decline within the first 5 cycles, experiencing greater losses at higher C-rates. However, at C/5 and C/10 the initial drop was less steep and a small increase in capacity was observed around 100 cycles, suggesting time-dependent dynamics of sulfur conversion. X-ray micro-CT imaging showed that significantly more active material was retained at a C/5 rate vs. 1C. We hope that this study provides a robust and "fail fast" platform for future investigations on electrode and electrolyte modifications. Strategies aimed at reducing conductive additive content, minimising and refining the electrolyte, and optimizing the management of sulfur species in redox reactions will be pivotal in realising the promise of ZELiS cells.

Acknowledgements

The authors acknowledge the support of The Faraday Institution's LiSTAR Programme (FIRG061). PRS was supported by the Department of Science, Innovation and Technology (DSIT) and the Royal Academy of Engineering under the Chair in Emerging Technologies programme (CiET1718/59).

References

[1] A. Bhargav, J. He, A. Gupta, A. Manthiram, Lithium-Sulfur Batteries: Attaining the Critical Metrics, Joule 4 (2020) 285–291. https://doi.org/10.1016/J.JOULE.2020.01.001.

[2] A. Manthiram, Y. Fu, S.H. Chung, C. Zu, Y.S. Su, Rechargeable lithium-sulfur batteries, Chem Rev 114 (2014) 11751–11787. https://doi.org/10.1021/cr500062v.

[3] S.H. Chung, C.H. Chang, A. Manthiram, Progress on the Critical Parameters for Lithium–Sulfur Batteries to be Practically Viable, Adv Funct Mater 28 (2018). https://doi.org/10.1002/adfm.201801188.

[4] K. Zhu, C. Wang, Z. Chi, F. Ke, Y. Yang, A. Wang, W. Wang, L. Miao, How Far Away Are Lithium-Sulfur Batteries From Commercialization?, Front Energy Res 7 (2019). https://doi.org/10.3389/fenrg.2019.00123.

[5] S.H. Chung, A. Manthiram, Designing Lithium-Sulfur Cells with Practically Necessary Parameters, Joule 2 (2018) 710–724. https://doi.org/10.1016/j.joule.2018.01.002.

[6] M. Wang, Z. Bai, T. Yang, C. Nie, X. Xu, Y. Wang, J. Yang, S. Dou, N. Wang, Advances in High Sulfur Loading Cathodes for Practical Lithium-Sulfur Batteries, Adv Energy Mater 12 (2022). https://doi.org/10.1002/aenm.202201585.

[7] H. Liu, W.H. Lai, Q. Yang, Y. Lei, C. Wu, N. Wang, Y.X. Wang, S.L. Chou, H.K. Liu, S.X. Dou, Understanding Sulfur Redox Mechanisms in Different Electrolytes for Room-

Temperature Na–S Batteries, Nanomicro Lett 13 (2021). https://doi.org/10.1007/s40820-021-00648-w.

[8] S. Nanda, A. Gupta, A. Manthiram, A Lithium–Sulfur Cell Based on Reversible Lithium Deposition from a Li2S Cathode Host onto a Hostless-Anode Substrate, Adv Energy Mater 8 (2018) 2–7. https://doi.org/10.1002/aenm.201801556.

[9] S. Nanda, A. Bhargav, A. Manthiram, Anode-free, Lean-Electrolyte Lithium-Sulfur Batteries Enabled by Tellurium-Stabilized Lithium Deposition, Joule 4 (2020) 1121–1135. https://doi.org/10.1016/j.joule.2020.03.020.

[10] J.B. Robinson, K. Xi, R.V. Kumar, A.C. Ferrari, H. Au, M.-M. Titirici, A. Parra-Puerto, A. Kucernak, S.D.S. Fitch, N. Garcia-Araez, Z.L. Brown, M. Pasta, L. Furness, A.J. Kibler, D.A. Walsh, L.R. Johnson, C. Holc, G.N. Newton, N.R. Champness, F. Markoulidis, C. Crean, R.C.T. Slade, E.I. Andritsos, Q. Cai, S. Babar, T. Zhang, C. Lekakou, N. Kulkarni, A.J.E. Rettie, R. Jervis, M. Cornish, M. Marinescu, G. Offer, Z. Li, L. Bird, C.P. Grey, M. Chhowalla, D. Di Lecce, R.E. Owen, T.S. Miller, D.J.L. Brett, S. Liatard, D. Ainsworth, P.R. Shearing, 2021 roadmap on lithium sulfur batteries, Journal of Physics: Energy 3 (2021) 031501. https://doi.org/10.1088/2515-7655/abdb9a.

[11] G. Li, X. Wang, M.H. Seo, M. Li, L. Ma, Y. Yuan, T. Wu, A. Yu, S. Wang, J. Lu, Z. Chen, Chemisorption of polysulfides through redox reactions with organic molecules for lithium–sulfur batteries, Nature Communications 2018 9:1 9 (2018) 1–10. https://doi.org/10.1038/s41467-018-03116-z.

[12] C. Deng, Z. Wang, S. Wang, J. Yu, Inhibition of polysulfide diffusion in lithium-sulfur batteries: Mechanism and improvement strategies, J Mater Chem A Mater 7 (2019) 12381–12413. https://doi.org/10.1039/c9ta00535h.

[13] S. Nanda, A. Gupta, A. Manthiram, Anode-Free Full Cells: A Pathway to High-Energy Density Lithium-Metal Batteries, Adv Energy Mater 11 (2021). https://doi.org/10.1002/AENM.202000804.

[14] X. Yu, A. Manthiram, Electrode-electrolyte interfaces in lithium-based batteries, Energy Environ Sci 11 (2018) 527–543. https://doi.org/10.1039/c7ee02555f.

[15] X.B. Cheng, Q. Zhang, Dendrite-free lithium metal anodes: Stable solid electrolyte interphases for high-efficiency batteries, J Mater Chem A Mater 3 (2015) 7207–7209. https://doi.org/10.1039/c5ta00689a.

[16] M. Zhao, B.Q. Li, X.Q. Zhang, J.Q. Huang, Q. Zhang, A Perspective toward Practical Lithium-Sulfur Batteries, ACS Cent Sci 6 (2020) 1095–1104. https://doi.org/10.1021/ACSCENTSCI.0C00449/ASSET/IMAGES/LARGE/OC0C00449_0005.JPEG.

[17] M. Wild, L. O'Neill, T. Zhang, R. Purkayastha, G. Minton, M. Marinescu, G.J. Offer, Lithium sulfur batteries, a mechanistic review, Energy Environ Sci 8 (2015) 3477–3494. https://doi.org/10.1039/c5ee01388g.

[18] ROADMAP • OPEN ACCESS You may also like, (2021).

[19] Y. Yang, G. Zheng, S. Misra, J. Nelson, M.F. Toney, Y. Cui, High-capacity micrometer-sized Li 2S particles as cathode materials for advanced rechargeable lithium-ion batteries, J Am Chem Soc 134 (2012) 15387–15394. https://doi.org/10.1021/JA3052206/SUPPL_FILE/JA3052206_SI_001.PDF.

[20] H. Ye, M. Li, T. Liu, Y. Li, J. Lu, Activating Li2S as the Lithium-Containing Cathode in Lithium-Sulfur Batteries, ACS Energy Lett 5 (2020) 2234–2245. https://doi.org/10.1021/ACSENERGYLETT.0C00936/ASSET/IMAGES/LARGE/NZ0C00936_0007.JPEG.

[21] J. Chen, J. Xiang, X. Chen, L. Yuan, Z. Li, Y. Huang, Li2S-based anode-free full batteries with modified Cu current collector, Energy Storage Mater 30 (2020) 179–186. https://doi.org/10.1016/J.ENSM.2020.05.009.

[22] C. Zhang, Q. Lan, Y. Liu, J. Wu, H. Shao, H. Zhan, Y. Yang, A dual-layered artificial solid electrolyte interphase formed by controlled electrochemical reduction of LiTFSI/DME-LiNO 3 for dendrite-free lithium metal anode, Electrochim Acta 306 (2019) 407–419. https://doi.org/10.1016/j.electacta.2019.03.162.

[23] R. Weber, M. Genovese, A.J. Louli, S. Hames, C. Martin, I.G. Hill, J.R. Dahn, Long cycle life and dendrite-free lithium morphology in anode-free lithium pouch cells enabled by a dual-salt liquid electrolyte, Nature Energy 2019 4:8 4 (2019) 683–689. https://doi.org/10.1038/s41560-019-0428-9.

[24] M. Agostini, J.-Y. Hwang, H.M. Kim, P. Bruni, S. Brutti, F. Croce, A. Matic, Y.-K. Sun, Minimizing the Electrolyte Volume in Li–S Batteries: A Step Forward to High Gravimetric Energy Density, Adv Energy Mater 8 (2018) 1801560. https://doi.org/10.1002/AENM.201801560.

[25] P. Vadhva, J. Hu, M.J. Johnson, R. Stocker, M. Braglia, D.J.L. Brett, A.J.E. Rettie, Electrochemical Impedance Spectroscopy for All-Solid-State Batteries: Theory, Methods and Future Outlook, ChemElectroChem 8 (2021) 1930–1947. https://doi.org/10.1002/CELC.202100108.

[26] S. Nanda, A. Manthiram, Lithium degradation in lithium-sulfur batteries: Insights into inventory depletion and interphasial evolution with cycling, Energy Environ Sci 13 (2020) 2501–2514. https://doi.org/10.1039/d0ee01074j.

[27] K. Cai, M.K. Song, E.J. Cairns, Y. Zhang, Nanostructured Li2S-C composites as cathode material for high-energy lithium/sulfur batteries, Nano Lett 12 (2012) 6474–6479. https://doi.org/10.1021/nl303965a.

[28] L.K.J. Ting, Y. Gao, H. Wang, T. Wang, J. Sun, J. Wang, Lithium Sulfide Batteries: Addressing the Kinetic Barriers and High First Charge Overpotential, ACS Omega 7 (2022) 40682–40700. https://doi.org/10.1021/acsomega.2c05477.

[29] N. Sabi, K. Palanisamy, F. Rahide, S. Daboss, C. Kranz, S. Dsoke, Surface Properties-Performance Relationship of Aluminum Foil as Negative Electrode for Rechargeable Aluminum Batteries, Batter Supercaps 6 (2023). https://doi.org/10.1002/batt.202300298.

[30] A. Robba, M. Mežnar, A. Vizintin, J. Bitenc, J. Bobnar, I. Arčon, A. Randon-Vitanova, R. Dominko, Role of Cu current collector on electrochemical mechanism of Mg–S battery, J Power Sources 450 (2020). https://doi.org/10.1016/j.jpowsour.2019.227672.

[31] K. Coke, M.J. Johnson, J.B. Robinson, A.J.E. Rettie, T.S. Miller, P.R. Shearing, Illuminating Polysulfide Distribution in Lithium Sulfur Batteries; Tracking Polysulfide Shuttle Using Operando Optical Fluorescence Microscopy, ACS Appl Mater Interfaces 16 (2023). https://doi.org/10.1021/ACSAMI.3C14612/SUPPL_FILE/AM3C14612_SI_001.PDF.

[32] J. Brückner, S. Thieme, H.T. Grossmann, S. Dörfler, H. Althues, S. Kaskel, Lithium–sulfur batteries: Influence of C-rate, amount of electrolyte and sulfur loading on cycle performance, J Power Sources 268 (2014) 82–87. https://doi.org/10.1016/J.JPOWSOUR.2014.05.143.

[33] A. Vizintin, L. Chabanne, E. Tchernychova, I. Arčon, L. Stievano, G. Aquilanti, M. Antonietti, T.P. Fellinger, R. Dominko, The mechanism of Li2S activation in lithium-sulfur batteries: Can we avoid the polysulfide formation?, J Power Sources 344 (2017) 208–217. https://doi.org/10.1016/J.JPOWSOUR.2017.01.112.

[34] R. Xu, I. Belharouak, X. Zhang, R. Chamoun, C. Yu, Y. Ren, A. Nie, R. Shahbazian-Yassar, J. Lu, J.C.M. Li, K. Amine, Insight into sulfur reactions in Li-S batteries, ACS Appl Mater Interfaces 6 (2014) 21938–21945. https://doi.org/10.1021/AM504763P/SUPPL_FILE/AM504763P_SI_001.PDF.

[35] C.N. Lin, W.C. Chen, Y.F. Song, C.C. Wang, L.D. Tsai, N.L. Wu, Understanding dynamics of polysulfide dissolution and re-deposition in working lithium–sulfur battery by in-operando transmission X-ray microscopy, J Power Sources 263 (2014) 98–103. https://doi.org/10.1016/J.JPOWSOUR.2014.04.003.

[36] L. Zielke, C. Barchasz, S. Walu, F. Alloin, J.C. Leprêtre, A. Spettl, V. Schmidt, A. Hilger, I. Manke, J. Banhart, R. Zengerle, S. Thiele, Degradation of Li/S battery electrodes on 3D current collectors studied using x-ray phase contrast tomography, Sci Rep 5 (2015). https://doi.org/10.1038/srep10921.

[37] A. Yermukhambetova, C. Tan, S.R. Daemi, Z. Bakenov, J.A. Darr, D.J.L. Brett, P.R. Shearing, Exploring 3D microstructural evolution in Li-Sulfur battery electrodes using in-situ X-ray tomography, Sci Rep 6 (2016). https://doi.org/10.1038/srep35291.

[38] X. Qiu, Q. Hua, L. Zheng, Z. Dai, Study of the discharge/charge process of lithium-sulfur batteries by electrochemical impedance spectroscopy, RSC Adv 10 (2020) 5283–5293. https://doi.org/10.1039/c9ra10527a.

[39] M. Gerle, N. Wagner, J. Häcker, M. Nojabaee, K.A. Friedrich, Identification of the Underlying Processes in Impedance Response of Sulfur/Carbon Composite

Cathodes at Different SOC, J Electrochem Soc 169 (2022) 030505. https://doi.org/10.1149/1945-7111/ac56a4.

[40] R. Soni, J.B. Robinson, P.R. Shearing, D.J.L. Brett, A.J.E. Rettie, T.S. Miller, Lithium-sulfur battery diagnostics through distribution of relaxation times analysis, Energy Storage Mater 51 (2022) 97–101. https://doi.org/10.1016/j.ensm.2022.06.016.

[41] A. Gupta, A. Bhargav, A. Manthiram, Highly Solvating Electrolytes for Lithium–Sulfur Batteries, Adv Energy Mater 9 (2019). https://doi.org/10.1002/aenm.201803096.

[42] P. Vadhva, T.E. Gill, J.H. Cruddos, S. Said, M. Siniscalchi, S. Narayanan, M. Pasta, T.S. Miller, A.J.E. Rettie, Engineering Solution-Processed Non-Crystalline Solid Electrolytes for Li Metal Batteries, Chemistry of Materials 35 (2023) 1168–1176. https://doi.org/10.1021/acs.chemmater.2c03071.